Wärme- und Stoffübertragung 27, 131–140 (1992)

Wärme- und Stoffübertragung

Thermal boundary condition effects on heat transfer in turbulent rough-wall boundary layers

R. P. Taylor, M. H. Hosni, J. W. Garner, and **H. W. Coleman,** Mississippi State, MS, USA

Abstract. Measurements and predictions are presented which investigate the effects of thermal boundary condition on heat transfer in the turbulent rough-wall boundary layer. Stanton number measurements are reported for the turbulent flow of air over rough plates with a variety of thermal boundary conditions on two separate rough surfaces. The cases considered are constant wall temperature, constant wall heat flux, step wall temperature, and piecewise linear wall temperature distributions. These measurements and data from other sources are compared with predictions using finite difference solutions of the discrete element roughness model and with superposition solutions. The predictions and the measurements are in good to excellent agreement.

Einfluß der thermischen Randbedingungen auf die Wärmeübertragung in turbulenten Grenzschichten an rauhen Wänden

Zusammenfassung. In dieser Arbeit werden Messungen und Berechnungen gezeigt, die den Einfluß der thermischen Randbedingungen auf die Wärmeübertragung in turbulenten Grenzschichten an rauhen Wänden untersuchen. Es werden Messungen der Stanton Zahl für turbulente Luftströmung über rauhe Platten an zwei separaten Oberflächen unter einer Reihe von thermischen Randbedingungen dargestellt. Die betrachteten Fälle sind konstante Wandtemperatur, konstanter Wärmestrom durch die Wand, abgestufte Wandtemperatur und stückweise konstante Wandtemperatur. Diese Messungen, sowie Daten anderer Untersuchungen, werden mit Berechnungen durch Finite-Differenzen Lösungen des Diskrete-Elemente-Rauhheits-Modells und Superpositionslösungen verglichen. Berechnungen und Messungen liegen in guter bis ausgezeichneter Übereinstimmung.

Nomenclature

A	plate surface area
a_j	parameter in Eq. (17)
b_i	finite step in wall temperature; Eq. (17)
C_D	roughness element drag coefficient
C_f	skin friction coefficient
C_p	specific heat
d_0	roughness element base diameter
$d(y)$	local roughness element diameter
$g(\xi, x)$	kernel function in Eq. (20)
H	enthalpy
$H_{0,\infty}$	freestream total enthalpy
$h(\xi, x)$	kernel function in Eq. (16) $= \varrho\, C_p\, U_\infty\, St(x, \xi)$
k	roughness element height
K	roughness element thermal conductivity
l_m	mixing length
L	roughness element spacing
m_j	slope in piecewise linear wall temperature variation; Eq. (17)
M	number of ramps in Eq. (17)
N	number of steps in Eq. (17)
Nu_d	roughness element Nusselt number
P	pressure
Pr	Prandtl number
Pr_t	turbulent Prandtl number
q_c	conductive heat loss rate
q_r	radiative heat loss rate
q''_w	wall heat flux
r	recovery factor
Re_d	Reynolds number based on local roughness element diameter
Re_x	x-Reynolds number
St	Stanton number
St_t	Stanton number for constant wall temperature
T	local fluid static temperature
T_0	freestream stagnation temperature
T_r	freestream recovery temperature
T_R	roughness element temperature
T_w	wall (plate) temperature
$\overline{u}$	mean longitudinal velocity
$\overline{u'v'}$	Reynolds shear stress factor
U_∞	freestream velocity
$(\overline{UA})_{\text{eff}}$	effective overall conductance for q_c calculation
$\overline{v'h'}$	turbulent heat flux factor
v	mean normal velocity
W	plate heater power
x	axial distance from nozzle exit
y	coordinate normal to surface
y^+	y-plus; $y\, U_\infty \sqrt{C_f/2}/\nu$

Greek symbols

$\beta_x(a, b)$	incomplete beta function
β_x	blockage factor
β_y	blockage factor
$\Gamma(x)$	gamma function
δ	boundary layer thickness
ε	plate surface emissivity
μ	viscosity
ν	kinematic viscosity
ξ	integration parameter
ϱ	density
ϕ	unheated length

Subscripts

t	turbulent
w	wall
∞	freestream

1 Introduction

Heat transfer can be significantly larger for turbulent flow over a rough surface compared with an equivalent turbulent flow over a smooth surface. Many surfaces of engineering interest involve convective heat transfer problems with aerodynamically rough surfaces. Turbine blades, reentry vehicles, atmospheric flows, and heat exchangers are examples of systems in which surface roughness can play an important role in heat transfer. The thermal boundary conditions for these situations are not always the constant wall temperature case. Therefore, it is important to understand and to be able to predict the effect of thermal boundary condition on convective heat transfer with a rough surface.

The effect of thermal boundary condition on heat transfer in the turbulent smooth-wall boundary layer has been extensively studied. The first systematic experimental study of this problem was the one of Reynolds, Kays, and Kline [1]. They measured the Stanton number for a variety of thermal boundary conditions with x-Reynolds numbers up to 3,500,000. Among the cases that they considered were constant wall temperature, constant wall heat flux, step wall temperature, arbitrary wall temperature, and arbitrary wall heat flux. They used this extensive data base to finalize the theory based on the integral solution of the boundary layer equations and the superposition of the energy equation solutions. Their work is still the definitive work in this area.

The smooth-wall results of Reynolds et al. have recently been extended to x-Reynolds numbers approaching 10,000,000 by P. H. Love and the present authors [2–6]. Heat transfer in the turbulent smooth-wall boundary layer was studied experimentally for constant wall temperature, constant wall heat flux, step wall temperature, step wall heat flux, and linear and bilinear wall temperature variations, and it was shown that the theory of Reynolds et al. readily extends to the higher Reynolds numbers. In addition, routine finite difference solutions of the time averaged boundary layer equations, such as those discussed by Cebeci and Bradshaw [7], include the effects of variable thermal boundary conditions very well. Taylor et al. [3–5] showed that these solutions are in good agreement with the data for a variety of thermal boundary conditions.

The effects of thermal boundary condition on convective heat transfer with rough surfaces have not been extensively studied. Coleman and his coworkers [8, 9] studied the effects of step wall temperature and linear and bilinear wall temperature variations for a rough surface comprised of 1.27 mm diameter spheres packed in the most dense array. They developed a solution method based on their data and the superposition theorem which was a modification of that of Reynolds et al. Ligrani [10] studied heat transfer in turbulent flow with the same roughness as Coleman but with artificially thickened boundary layers. Therefore, his data included an effective unheated starting length because of the virtual origin of the thickened momentum boundary layer. Ligrani also developed a prediction method based on the finite difference solution of the time averaged boundary layer equations. He used an adaptation of the modified mixing length model – much like that of Cebeci and Chang [11] – based on equivalent sandgrain roughness concepts.

The present authors (Taylor et al. [12, 13]) reported a comparison of Stanton number measurements with constant wall temperature and constant wall heat flux boundary conditions for turbulent flow over rough surfaces [12] and a study of the effects of step-wall temperature boundary conditions on rough surfaces [13]. They found that, when plotted as the ratio of Stanton number to constant wall temperature Stanton number, St/St_t, the data for both rough and smooth surfaces scatter about a single curve. The step-wall temperature data were used to formulate a new kernel function for use in the superposition solution of the arbitrary wall temperature problem.

The experiments reported in this paper were designed to investigate the effects of thermal boundary condition on heat transfer in the turbulent rough-wall boundary layer and to provide test cases for the prediction methods. Stanton number measurements were made for the turbulent flow of air over rough plates with a variety of thermal boundary conditions on two separate rough surfaces. The cases considered were constant wall temperature, constant wall heat flux, step wall temperature, and piecewise linear wall temperature distributions. Some of this data has been reported elsewhere [12, 13] and some of it is reported here for the first time. These measurements and the variable wall temperature data of Coleman [8] are compared with the discrete element model (Taylor, Coleman, and Hodge [14]) predictions and with predictions using the superposition solution with the step wall temperature kernel function of Taylor et al. [13].

2 Experimental apparatus and measurement procedures

2.1 Apparatus

The experiments were performed in the Turbulent Heat Transfer Test Facility (THTTF) which is shown schematically in Fig. 1. Complete descriptions of the facility and its qualification are presented in Coleman et al. [15]. This facility is a closed loop wind tunnel with a freestream velocity range of 6 to 67 m/s. The temperature of the circulating air is controlled with an air to water heat exchanger and a cooling water loop. Following the heat exchanger the air flow is conditioned by a system of honeycomb and screens.

The bottom wall of the nominally 2.4 m long by 0.5 m wide by 0.1 m high test section consists of 24 electrically

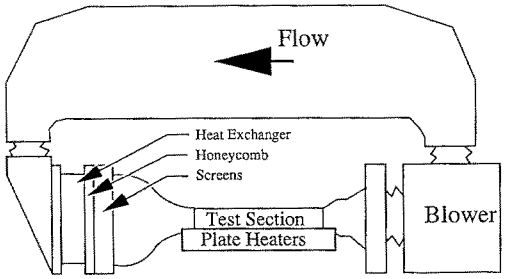

Fig. 1. Schematic diagram of the Turbulent Heat Transfer Test Facility (THTTF)

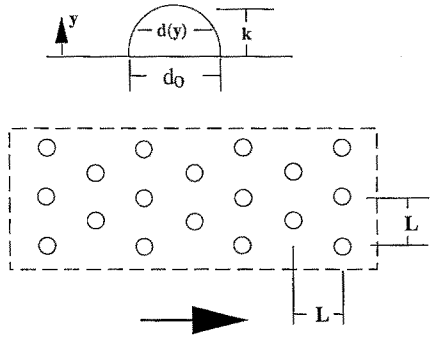

Fig. 2. Schematic diagram and layout of the surface roughness

heated flat plates which are abutted together to form a flat surface. The allowable step or mismatch between any two plates is 0.0013 cm. Each nickel plated aluminum plate (about 10 mm thick by 0.1 m in the flow direction) is uniformly heated from below by a custom-manufactured, rubber-encased electric heater pad. Design computations showed that, with this configuration, a plate can be considered to be at a uniform temperature. The heating system is under active computer control and any desired set of plate temperatures can be maintained within the limits of the power supply. To minimize the conduction losses, the side rails which support the plates are heated to approximately the same temperature as the plates.

The top wall can be adjusted to maintain a constant freestream velocity. An inclined water manometer with a resolution of 0.06 mm is used to measure the pressure gradient during top wall adjustment. Static pressure taps are located in the side wall adjacent to each plate. The pressure tap located at the second plate is used as a reference, and the pressure difference between it and each other tap is minimized. For example, the maximum pressure difference for a freestream velocity of 42 m/s was 0.30 mm of water compared with the freestream velocity head of about 100 mm of water.

The boundary layer is tripped at the exit of the 19 : 1 area ratio inlet nozzle with a 1 mm × 12 mm wooden strip. This trip location is immediately in front of the heated surface.

Two separate sets of rough surface plates were used in these experiments. Each rough plate was precision machined from a solid piece of aluminum using a specially designed diamond tool. A precision numerically controlled milling machine was used to mill out an array of cubes. The special diamond tool was then used to form the cubes into hemispheres. The finished plates were then nickel plated. The result was a very smooth flat surface with a staggered array of hemispherical roughness elements with a base diameter $d_0 = 1.27$ mm as shown in Fig. 2. The measured average roughness on the "smooth" wall portion of the plates with $L/d_0 = 4$ is less than 1.6 μm. The surface finish on the plates with $L/d_0 = 2$ is visually smooth – the same appearance as the $L/d_0 = 4$ surface. However, the finish was not measured because the available profilometer stylus would not fit between the rows. The surface with $L/d_0 = 4$ has a surface area to plan area ratio of about 1.05, and the $L/d_0 = 2$ surface has a ratio of about 1.20.

Since the roughness elements and the base plate are a continuous piece of aluminum, the thermal contact between the elements and the base is perfect. For the conditions of these experiments, design calculations showed that each plate and its roughness elements can be considered to be at a uniform temperature.

Before proceeding with the testing, a series of smooth-wall qualification tests were performed to insure the fitness of the test rig and the correctness of the instrumentation and the data acquisition and reduction procedures [15]. Measurements in the nozzle exit plane showed the mean velocity to be uniform within about 0.5 percent and the freestream turbulence intensity to be less than 0.3 percent. Measurements 1.1 m downstream of the nozzle exit showed the spanwise variation of momentum thickness to be less than ±5 percent. Profiles of mean temperature and velocity were in good agreement with the usual "law-of-the-wall." Stanton number data for the constant wall temperature cases were in excellent agreement with the data of Reynolds et al. [1], which is the definitive data set on which the usual Stanton number correlations are based. The THTTF smooth-wall data fall within the data scatter of this definitive data set.

2.2 Stanton number determination

The data reduction expression for the experimentally determined Stanton number is

$$St = \frac{W - q_r - q_c}{A\,\varrho\,C_p\,U_\infty\,(T_w - T_0)} \tag{1}$$

The power, W, supplied to each plate heater is measured with a precision wattmeter. The radiation het loss rate, q_r, is estimated using a gray body enclosure model where the emissivity of the nickel plated aluminum is estimated as $\varepsilon = 0.11$. The conductive heat loss rate, q_c, is calculated using an experimentally determined effective plate conductance, $(UA)_{\text{eff}}$, which includes both side rail and back losses. The conduction losses are minimized by actively heating the side rails. Both q_r/W and q_c/W are generally in the 0.5 percent to 1 percent range. The plate plan area, A, is determined from the length and width dimensions. The density and specific

heat are determined from property data for moist air using the measured values of barometric pressure and wet and dry bulb temperatures in the tunnel. The freestream velocity is measured using a Pitot probe and specially calibrated precision pressure transducers. The plate and freestream temperatures are measured using specially calibrated thermistors. The plate temperatures, T_w, are measured using 2 thermistors installed in wells in the back of each plate using conducting paste. The freestream total temperature, T_0, is computed using the measured freestream recovery temperature, T_r, and a recovery factor for the freestream thermistor probe of $r=0.86$ (Eckert and Goldstein [16]). All fluid properties are evaluated at the freestream static temperature.

The uncertainty in the experimental Stanton number was estimated based on the ANSI/ASME Standard on Measurement Uncertainty [17] following the procedures of Coleman and Steele [18]. For the Stanton number data in this paper, the overall uncertainty, as discussed in detail in Coleman et al. [15], ranged from about ± 2 to ± 5 percent for the constant temperature cases and ± 3 to ± 6 percent for the other cases, depending on flow conditions.

The constant heat flux cases were obtained by heating each plate at the same rate. Since each plate was individually at a constant temperature, the actual boundary condition was a series of temperature steps that gave the same average heat flux value over each 0.1 m long plate. This approximated a true constant heat flux boundary condition. The exact effect of this approximation on these experiments is unknown. The smooth-wall cases were in good agreement with constant heat flux finite difference solutions of the Reynolds averaged boundary layer equations and in general agreement with other experiments [3]. Also, the results of the predictions using the constant heat flux boundary condition given in this paper for the rough-wall are in good agreement with the data.

Plate to plate conduction contributes to the uncertainty of the Stanton numbers in varying amounts. For the constant wall temperature cases, temperatures of neighboring plates are approximately equal and the effect of plate to plate conduction is negligible. All uncertainties have been calculated using this assumption. However, for the other boundary conditions, plate temperatures vary along the test section and plate to plate conduction contributes to the uncertainty of the Stanton number measurements. Conduction experiments and uncertainty calculations [2] indicate that an addition of 1 percent to the calculated uncertainty should account for the plate to plate conduction except for special plates such as the first heated plate in the step-temperature cases.

3 Prediction approaches

Two prediction approaches are considered here. The first is the finite difference solution of the boundary layer equations with the discrete element roughness model. The second is the superposition solution using the step wall temperature results [13] as a kernel function.

3.1 Discrete element method

The basic idea of the discrete element approach is to treat the roughness as a collection of individual entities and to account for blockage, form drag, and heat transfer on each element. The discrete element scheme used is formulated for roughness elements with three-dimensional shapes (as opposed to transverse ribs) for which the element cross section can be approximated as circular at every height, y. This scheme includes the physical effects of roughness on the flow field by considering the blockage effects of the roughness elements, the drag forces which the roughness elements exert on the field, and the local heat transfer between the roughness elements and the fluid. The steady (Reynolds-averaged), two-dimensional, turbulent boundary layer equations presented here are for flow over a rough surface with roughness elements of uniform spacing as formulated by Taylor et al. [14].

Mass:

$$\frac{\partial}{\partial x}(\varrho\,\beta_x\,u)+\frac{\partial}{\partial y}(\varrho\,\beta_y\,v)=0 \tag{2}$$

Momentum:

$$\beta_x\,\varrho\,u\frac{\partial u}{\partial x}+\beta_y\,\varrho\,v\frac{\partial u}{\partial y}=-\frac{\partial}{\partial x}(\beta_x P)+\frac{\partial}{\partial y}\left[\beta_y\left(\mu\frac{\partial u}{\partial y}-\overline{\varrho\,u'\,v'}\right)\right]-\frac{1}{2}\varrho\,C_D\,d(y)\frac{u^2}{L^2} \tag{3}$$

Energy:

$$\beta_x\,\varrho\,u\frac{\partial H}{\partial x}+\beta_y\,\varrho\,v\frac{\partial H}{\partial y}=\frac{\partial}{\partial y}\left[\beta_y\left(\frac{K}{C_p}\frac{\partial H}{\partial y}-\overline{\varrho\,v'\,h'}\right)\right]+u\frac{\partial}{\partial x}(\beta_x P)+\beta_y\frac{\partial u}{\partial y}\left(\mu\frac{\partial u}{\partial y}-\overline{\varrho\,u'\,v'}\right)+\frac{1}{2}\varrho\,C_D\frac{d(y)}{L^2}u^3+\pi\frac{K\,Nu_d}{L^2}(T_R-T) \tag{4}$$

Empirical models for $-\varrho\,\overline{u'\,v'}$, $-\varrho\,\overline{v'\,h'}$, and the roughness element drag coefficient, C_D, and the roughness element Nusselt number, Nu_d, are necessary for closure. The blockage parameters, β_x and β_y, and the element shape descriptor, $d(y)$, require no empirical fluid mechanics input as they are determined solely from the geometry of the rough surface. Taylor et al. [14] have shown for uniform three-dimensional roughness elements with circular cross-section that

$$\beta_x=\beta_y=1-\frac{\pi\,d^2}{4\,L^2} \tag{5}$$

The boundary conditions for the discrete element approach for rough wall flows are identical to those for smooth wall flows. The wall location ($y=0$) is the smooth surface on

which the roughness elements occur. At $y=0$, $u=v=0$ and $H=H_w$. As $y \to \infty$, $u \to U_\infty$ and $H \to H_\infty$.

The "wall shear stress" is defined as the sum of the shear and drag forces on the wall in the mean flow direction divided by the plan area of the wall. The corresponding skin friction coefficient is

$$C_f = \frac{(\beta_y)_w \mu \left.\frac{\partial u}{\partial y}\right|_w + \frac{1}{2}\frac{1}{L^2}\int_0^\infty (\varrho\, dC_D\, u^2)\, dy}{\frac{1}{2}\varrho_\infty U_\infty^2} \tag{6}$$

and the Stanton number is

$$St = \frac{-(\beta_y)_w \frac{K}{C_p}\left.\frac{\partial H}{\partial y}\right|_w + \frac{\pi}{L^2}\int_0^\infty [K\, Nu_d\, (T_R - T)]\, dy}{\varrho_\infty U_\infty (H_w - H_{0,\infty})} \tag{7}$$

In order to solve Eqs. (2), (3), and (4), turbulence models and roughness models for C_D and Nu_d are required. Because of its wide acceptance and proven predictive capability for boundary layer flows over smooth surfaces, the Prandtl mixing length model with van Driest damping and a constant turbulent Prandtl number is used for turbulence closure. Thus

$$-\overline{\varrho\, u'\, v'} = \varrho\, l_m^2 \left(\frac{\partial u}{\partial y}\right)\left|\frac{\partial u}{\partial y}\right| = \mu_t \frac{\partial u}{\partial y} \tag{8}$$

where

$$l_m = 0.40\, y\, [1 - \exp(-y^+/26)]; \quad l_m < 0.09\, \delta \tag{9}$$

$$l_m = 0.09\, \delta; \quad \text{otherwise} \tag{10}$$

and

$$-\overline{\varrho\, v'\, h'} = \frac{\mu_t}{Pr_t}\frac{\partial H}{\partial y}; \quad Pr_t = 0.9 \tag{11}$$

Taylor et al. [14], as did Lin and Bywater [19], chose to formulate the roughness element C_D and Nu_d models as functions of the local element Reynolds number

$$Re_d = \frac{u(y)\, d(y)}{\nu} \tag{12}$$

which includes roughness element size and shape information through $d(y)$. As discussed in reference [14], the C_D model which gave the best overall agreement was

$$\log_{10}(C_D) = -0.125 \log_{10}(Re_d) + 0.375 \tag{13}$$

The C_D model has been tested for values of Re_d up to about 25,000 [14, 20].

Hosni, Coleman, and Taylor [21] recently reported a refined Nu_d model

$$Nu_d = 1.7\, Re_d^{0.49}\, Pr^{0.4} \tag{14}$$

which has been tested up to Re_d of about 2200 using several experimental runs from multiple rough surfaces.

The numerical solution of the discrete element equations is obtained by finite difference solution of the transformed equations in the computational plane. The transformation, finite difference scheme, and program structure [14] are very similar to those given by Gatlin and Hodge [22] for the smooth-wall. The streamwise derivative is approximated with a first-order backwards difference. The surface normal derivatives are replaced with second-order approximations which allow the spacing between grid points to vary with distance from the wall. This allows a concentration of nodes near the wall and below the crests of the elements. In this stretched grid the ratio of any two adjacent mesh lengths is a constant.

The solution is by an iterative marching, implicit method. The solution is known at station i and is sought at station $i+1$. The implicit difference equations result in a tridiagonal coefficient matrix whose inverse is known and can be expressed algebraically (often referred to as the Thomas algorithm). Since the equations are non-linear, the system must be solved by iteration. A relaxation scheme is employed with a required residual <0.01 percent.

The solutions were obtained on finer and finer grids until differences were less than 1 percent in computed values of C_f and St. However, a slight wiggle was observed in the solutions. This wiggle is caused by the occasional loss of a computational node below the crest of the elements as the gird expands in physical space to fill the growing boundary layer. This process is akin to a step change in the surface boundary condition. A similar wiggly result correctly models the response of the boundary layer to a step change in wall temperature. The amplitude and wavelength of the wiggles can be reduced by increasing the number of grid points if resources allow.

In addition, the codes were verified by comparisons with known solutions of smooth-wall laminar and turbulent flows.

3.2 Superposition

For constant property flow over a flat plate with constant freestream velocity and temperature, the problem of boundary layer heat transfer with arbitrary wall temperature can be solved by the method of superposition. The kernel function in this superposition is the result for a boundary layer with a step wall temperature boundary condition. Recently, Taylor et al. [13] have shown that for both smooth and rough surfaces the Stanton number for the turbulent flat plate boundary layer with unheated starting length, ϕ, can be expressed as

$$\frac{St(x;\phi)}{St_t(x)} = \left[1 - \left(\frac{\phi}{x}\right)^{0.677}\right]^{-0.13} \tag{15}$$

where St_t is the Stanton number for the isothermal plate with the same surface roughness and at the same freestream velocity.

Following the development of Reynolds et al. [1] for smooth surfaces, substitution of Eq. (15) into the superposition integral for a piecewise continuous wall temperature distribution with a finite number of steps

$$q''_w(x) = \int_0^x h(\xi; x) \frac{d(T_w - T_\infty)}{d\xi} d\xi + \sum_{i=1}^{N} h(\xi_i; x)\, \Delta(T_{wi} - T_\infty) \tag{16}$$

along with the formula for a piecewise linear wall temperature distribution

$$(T_w - T_\infty) = \sum_{j=1}^{M} m_j (x - a_j) + \sum_{i=1}^{N} b_i \tag{17}$$

gives the Stanton number for a piecewise linear T_w distribution

$$\frac{St(x)}{St_t(x)} = \frac{1.477\, x}{(T_w - T_\infty)} \sum_{j=1}^{M} m_j \beta_{r_j}(0.87, 1.477) + \frac{1}{(T_w - T_\infty)} \sum_{i=1}^{N} b_i \left[1 - \left(\frac{\xi_i}{x}\right)^{0.677}\right]^{-0.13} \tag{18}$$

where $\beta_{r_j}(0.87, 1.477)$ is the incomplete beta function with $(r_j = 1 - (a_j/x)^{0.677})$

$$\beta_r(a, b) = \int_0^r z^{a-1} (1-z)^{b-1}\, dz \tag{19}$$

The inverse problem, where the wall heat flux is specified, can be formulated as

$$(T_w - T_\infty) = \int_0^x g(\xi; x)\, q''_w(\xi)\, d\xi \tag{20}$$

Using Eq. (15) and following the development of Kays and Crawford [23] for smooth surfaces the kernel function, $g(\xi; x)$ is given by

$$g(\xi; x) = \frac{0.677}{\varrho\, U_\infty\, C_p\, St_t(x)\, x\, \Gamma(0.13)\, \Gamma(0.87)} \left[1 - \left(\frac{\xi}{x}\right)^{0.677}\right]^{-0.87} \tag{21}$$

or in terms of the local Stanton number

$$\frac{St_t(x)}{St(x)} = \frac{0.677}{x\, \Gamma(0.13)\, \Gamma(0.87)\, q''_w(x)} \int_0^x \left[1 - \left(\frac{\xi}{x}\right)^{0.677}\right]^{-0.87} q''_w(\xi)\, d\xi \tag{22}$$

For the special case of constant wall heat flux, Eq. (22) reduces to

$$\frac{St(x)}{St_t(x)} = \frac{\Gamma(0.13)\, \Gamma(0.87)}{\beta_1(0.13, 1.477)} = 1.1 \tag{23}$$

These solutions are very general but have the disadvantage of requiring prior knowledge of the Stanton number distribution for the isothermal case, $St_t(x)$. For smooth surfaces several good correlations are available (see Kays and Crawford [23] or Taylor et al. [3]). However for rough surfaces no general correlations exist and isothermal plate data must be available for the surface of interest at the same freestream velocity.

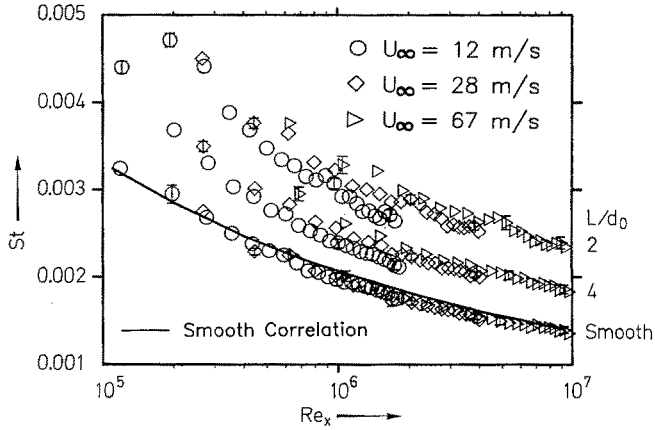

Fig. 3. Comparison of the constant wall temperature data for the smooth surface and the two rough surfaces, $U_\infty = 12$, 28, and 67 m/s

4 Results

Comparisons are made between the experimental results and the predictions for a variety of thermal boundary conditions on the two rough surfaces. Figure 3 shows selected data from Hosni et al. [21] for turbulent boundary layer flow over the two rough surfaces and a smooth surface with constant wall temperature boundary conditions at freestream velocities of $U_\infty = 12$, 28, and 67 m/s. This figure shows the influence of the roughness on the heat transfer level to be large. The $L/d_0 = 4$ surface Stanton number is about 40 percent greater than the smooth-wall value, and the $L/d_0 = 2$ surface Stanton number is about 75 percent greater than the smooth-wall value. The curve is the smooth wall Stanton number correlation expression from Taylor et al. [3]

$$St_t = 0.185\, Pr^{-0.4} [\log_{10}(Re_x)]^{-2.584} \tag{24}$$

which uses the classic Schultz-Grunow [24] expression for C_f. For the smooth-wall cases, the data for different freestream velocities collapse to a single curve in these coordinates which is in good agreement with the correlation. However, this is not the case for the rough surfaces.

For the $L/d_0 = 2$ surface at a Re_x of about 1,500,000, the Stanton numbers for the 67 m/s case are about 20 percent larger than the ones for the 12 m/s case. This behavior has been observed by others [8, 10] and is the expected behavior for rough-wall turbulent boundary layer heat transfer. It is related to the concept of aerodynamically smooth, transitionally rough, and fully rough flow regimes. This behavior is troublesome for the superposition solutions which require prior knowledge of the constant wall temperature Stanton number. Since the Stanton number data do not fall on a single curve over the entire range of freestream velocities,

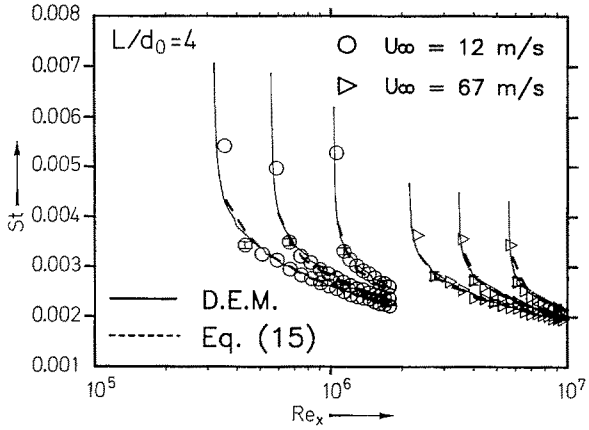

Fig. 4. Comparison of the step-wall temperature data with the discrete element predictions and Eq. (15) for the $L/d_0=4$ surface

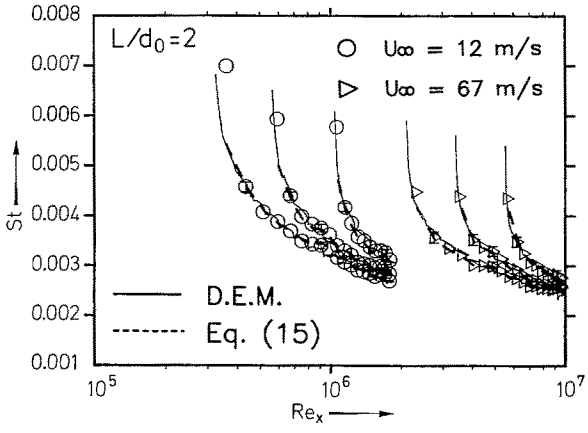

Fig. 5. Comparison of the step-wall temperature data with the discrete element predictions and Eq. (15) for the $L/d_0=2$ surface

simple explicit correlations such as Eq. (24) can not be formulated for rough surfaces. A more detailed discussion is outside the scope of this paper and is given by Hosni et al. [21]. For the $L/d_0=4$ surface, Hosni et al. classified the 12 m/s case as transitionally rough and the 28 and 67 m/s cases as fully rough. For $L/d_0=2$, the 12, 28, and 67 m/s cases were all classified as fully rough.

Figures 4 and 5 show the comparison between the predictions and the data for the step wall temperature boundary conditions for the $L/d_0=4$ and 2 rough surfaces, respectively. These conditions consisted of an unheated length followed by a constant temperature heated region. For the freestream velocity of 12 m/s, the unheated lengths were 0.4, 0.7, and 1.3 m. For the 67 m/s cases, they were 0.5, 0.8, and 1.3 m. Both the discrete element method solutions and Eq. (15) are in excellent agreement with the data. It should be pointed out, though, that Eq. (15) was determined from a curve-fit using these data.

Figures 6 and 7 show the comparison of the discrete element method predictions with the constant heat flux data for the $L/d_0=4$ and 2 rough surfaces, respectively. As mentioned previously, the constant heat flux boundary conditions were approximated by a series of 0.1 m long constant wall temperature steps. The solid curves show the results of the computations using the measured wall temperature distributions modeled as a series of steps for the boundary

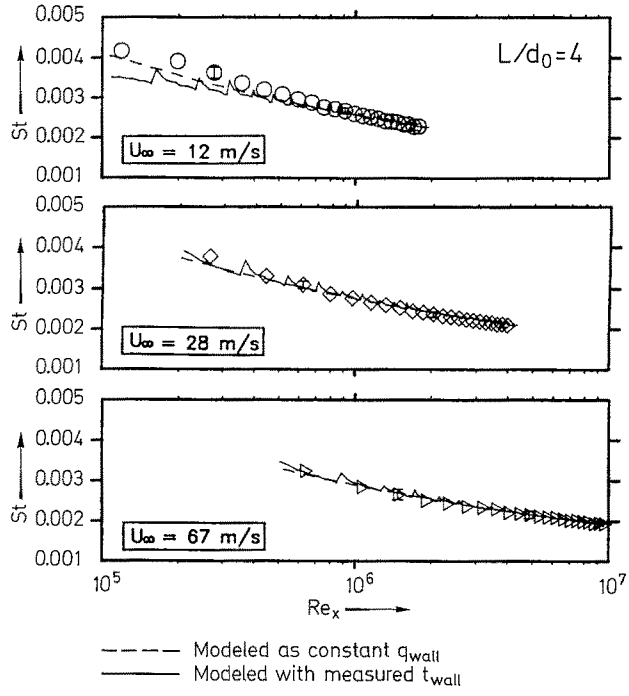

Fig. 6. Comparison of the constant heat flux data with the discrete element predictions for the $L/d_0=4$ surface

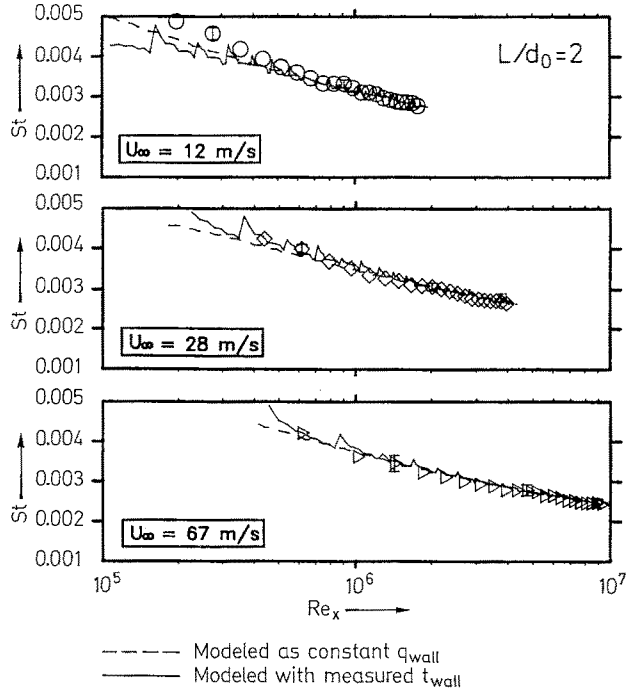

Fig. 7. Comparison of the constant heat flux data with the discrete element predictions for the $L/d_0=2$ surface

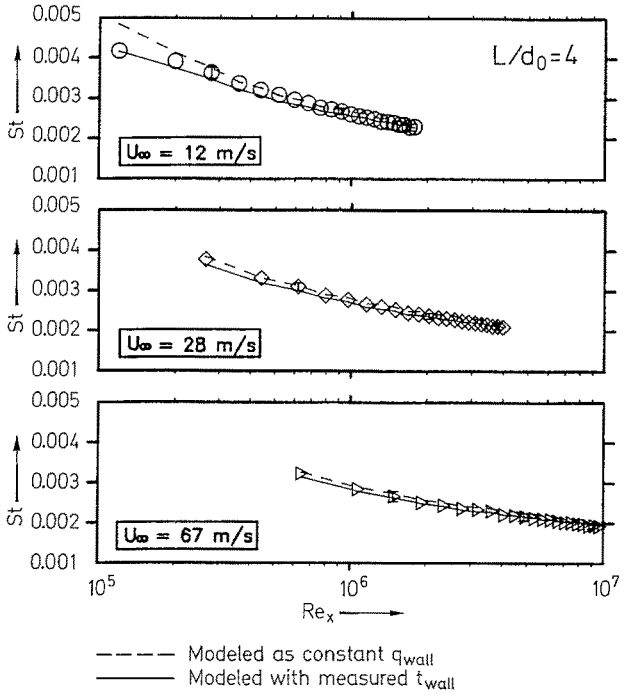

Fig. 8. Comparison of the constant heat flux data with the superposition solutions for the $L/d_0 = 4$ surface

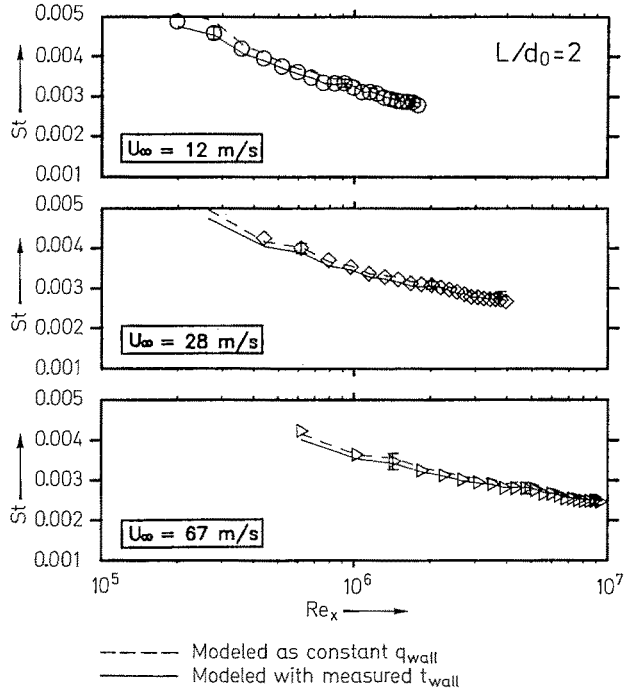

Fig. 9. Comparison of the constant heat flux data with the superposition solutions for the $L/d_0 = 2$ surface

conditions. The saw-tooth nature of the solutions is a result of the steps in temperature at the plate interfaces. The dashed curves show the computations using constant heat flux boundary conditions. The two solutions are in general in very good agreement with each other and with the data. The exceptions are the first few plates for $U_\infty = 12$ m/s. Uncertainty bars are included on representative data points and the symbol size is in most cases representative of the uncertainty.

Figures 8 and 9 show the same comparison for the superposition solutions. The solid curves were computed using Eq. (18) with measured wall temperature distributions and the corresponding constant wall temperature Stanton number, St_t, measured by Hosni et al. [21]. The dashed curves were computed using Eq. (23) and the measured St_t distributions. The two solutions are in very good agreement with each other and with the data. The exceptions are the first few plates for $U_\infty = 12$ m/s.

The comparisons in Figures 6–9 indicate that the step wall temperature approximation of the constant wall heat flux boundary condition is appropriate for the conditions of these experiments.

Figures 10 and 11 show comparisons of the discrete element method and superposition solutions, respectively, and data from the $L/d_0 = 4$ rough surface for linear and bilinear wall temperature distributions. The linear distributions consist of a series of steps where the plate temperature decreases nominally 0.5 °C from plate to plate. The bilinear distributions consist of a series of nominal 0.5 °C decreases in plate temperature followed by a series of 0.5 °C increases.

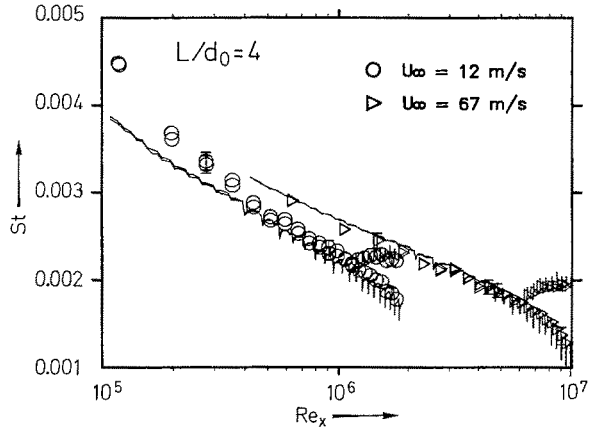

Fig. 10. Comparison of the linear and bilinear wall temperature data with the discrete element predictions for the $L/d_0 = 4$ surface

Figure 10 shows the comparison for the discrete element method solutions. The thermal boundary conditions used in the computations were the measured wall temperatures modeled as a series of steps. As before, the saw-tooth effect is a result of the step in wall temperature at the plate interfaces. The agreement between the solutions and the data is excellent. The exceptions are again for the first few plates at $U_\infty = 12$ m/s. Figure 11 shows the same comparison for the superposition solutions. The computations were made using Eq. (18) with the measured wall temperatures modeled as a series of steps and with the corresponding St_t measurements. The agreement is excellent.

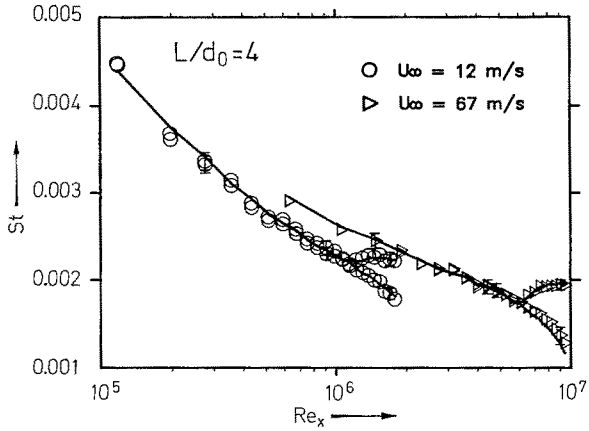

Fig. 11. Comparison of the linear and bilinear wall temperature data with the superposition solutions for the $L/d_0 = 4$ surface

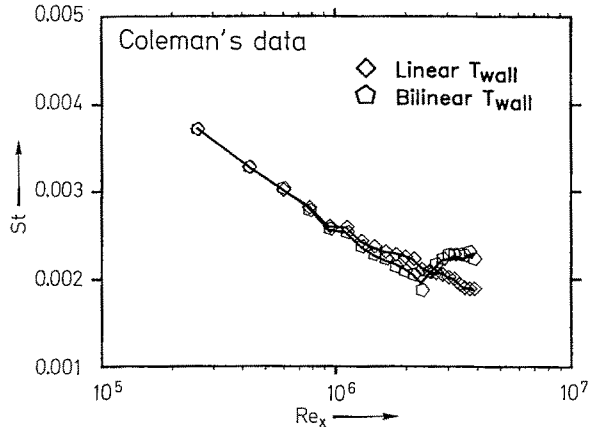

Fig. 13. Comparison of the linear and bilinear wall temperature data with the superposition solutions for Coleman's [8] surface

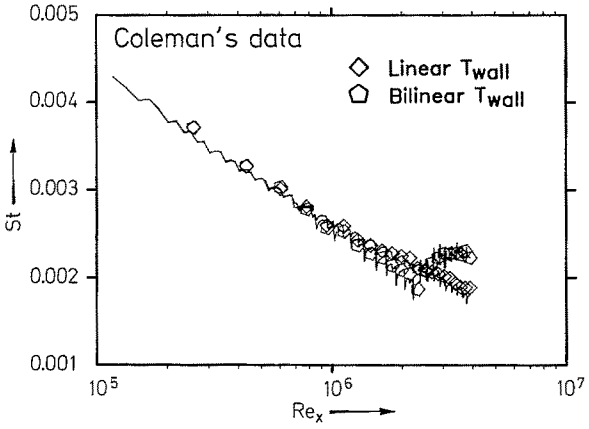

Fig. 12. Comparison of the linear and bilinear wall temperature data with the discrete element predictions for Coleman's [8] surface

In the comparisons above, the St data from the first few plates in the 12 m/s cases consistently showed agreement which was poorer than the excellent agreement seen elsewhere. Even though the boundary layer was tripped at the nozzle exit and the surfaces were very rough, the flow over the first few plates at $U_\infty = 12$ m/s was not fully turbulent. All of the prediction schemes assumed fully turbulent flow. The comparisons in Figures 8, 9, and 11 show that the superposition solutions using the measured wall temperatures and St_t are in better agreement with the data. This is a result of latent information on the state of the boundary layer contained in T_w and St_t.

Figures 12 and 13 show comparisons of the discrete element method and superposition solutions, respectively, with the rough-wall Stanton number data of Coleman [8] for both linear and bilinear wall temperature variations. This surface was comprised of 1.27 mm diameter spheres packed in the most dense array. The experiments were performed in a wind tunnel facility which was very much like the facility described in this paper. According to Coleman, the boundary layer was fully rough in both cases. The linear distribution consisted of a series of nominal 0.4 °C step decreases. The bilinear distribution consisted of a series of nominal 0.8 °C decreases followed by 0.8 °C increases. Figure 12 shows the comparison with the discrete element solutions with the wall temperature distribution modeled as a series of steps. Figure 13 shows the comparison with the superposition solutions using Coleman's measured values of St_t. The agreement is seen to be excellent.

5 Summary

Heat transfer measurements and predictions are presented for turbulent rough-wall boundary layers with a variety of thermal boundary conditions. The predictions using both the discrete element method and the superposition solution are in good to excellent agreement with the experiments. The superposition solutions are general but have the disadvantage of requiring constant wall temperature heat transfer data from the same or a similar rough surface at the same freestream velocity. On the other hand, the finite difference solutions using the discrete element method are more truly predictions and do not require previous knowledge of the heat transfer on the surface.

The rough-wall experiments reported in this paper were all performed using uniform arrays of hemispherical elements. It is the authors' opinion that the trends reported here should be generally valid. However, if this is to be demonstrated, additional variable thermal boundary condition experiments using a variety of rough surfaces are required.

Acknowledgements

This work was supported by the U.S. Air Force Office of Scientific Research (Research Grant AFOSR-86-0178); the experimental apparatus was acquired under grant AFOSR-85-0075. The authors gratefully acknowledge the interest and encouragement of Capt. Hank Helin of AFOSR.

References

1. Reynolds, W. C.; Kays, W. M.; Kline, S. J.: Heat transfer in the turbulent incompressible boundary layer. Parts I, II, and III, NASA MEMO 12-1-58W, 12-2-58W, 12-3-58W, 1958
2. Love, P. H.; Taylor, R. P.; Coleman, H. W.; Hosni, M. H.: Effects of thermal boundary condition on heat transfer in the turbulent incompressible flat plate boundary layer. Report TFD-88-3, Mechanical and Nuclear Engineering Department, Mississippi State University, 1988
3. Taylor, R. P.; Coleman, H. W.; Hosni, M. H.; Love, P. H.: Thermal boundary condition effects on heat transfer in the turbulent incompressible flat plate boundary layer. Int. J. Heat Mass Transfer 32 (1989) 1165–1174
4. Taylor, R. P.; Love, P. H.; Coleman, H. W.; Hosni, M. H.: Step heat flux effects on turbulent boundary layer heat transfer. AIAA J. Thermophysics and Heat Transfer 4 (1990) 121–123
5. Taylor, R. P.; Love, P. H.; Coleman, H. W.; Hosni, M. H.: Heat transfer measurements in incompressible turbulent flat plate boundary layers with step wall temperature boundary conditions. ASME J. Heat Transfer 112 (1990) 245–247
6. Taylor, R. P.; Love, P. H.; Coleman, H. W.; Hosni, M. H.: The effects of step changes in thermal boundary condition on heat transfer in the incompressible flat plate turbulent boundary layer. In: Heat Transfer in Convective Flows, ASME HTD-Vol. 107 (1989) 9–16
7. Cebeci, T.; Bradshaw, P.: Physical and computational aspects of convective heat transfer. New York: Springer 1984
8. Coleman, H. W.: Momentum and energy transport in the accelerated fully rough turbulent boundary layer. Ph.D. Dissertation, Mechanical Engineering Department, Stanford University, 1976 (also Report HMT-24)
9. Coleman, H. W.; Pimenta, M. M.; Moffat, R. J.: Rough-wall turbulent heat transfer with variable velocity, wall temperature, and blowing. AIAA J. 16 (1978) 78–82
10. Ligrani, P. M.: The thermal and hydrodynamic behavior of thick, rough-wall, turbulent boundary layers. Ph.D. Dissertation, Mechanical Engineering Department, Stanford University, 1979 (also Report HMT-29)
11. Cebeci, T.; Chang, K. C.: Calculation of incompressible rough-wall boundary layer flows. AIAA J. 16 (1978) 730–735
12. Taylor, R. P.; Hosni, M. H.; Coleman, H. W.: Comparison of constant wall temperature and heat flux cases for the turbulent rough-wall boundary layer. Experimental Heat Transfer 3 (1990) 117–127
13. Taylor, R. P.; Hosni, M. H.; Garner, J. W.; Coleman, H. W.: Rough-wall turbulent heat transfer with step wall temperature boundary conditions. AIAA paper 90-1501 presented at the AIAA 21st Fluid Dynamics, Plasmadynamics and Lasers Conference, 1990
14. Taylor, R. P.; Coleman, H. W.; Hodge, B. K.: A discrete element prediction approach for turbulent flow over rough surfaces. Report TFD-84-1, Mechanical and Nuclear Engineering Department, Mississippi State University, 1984
15. Coleman, H. W.; Hosni, M. H.; Taylor, R. P.; Brown, G. B.: Smooth wall qualification of a turbulent heat transfer test facility. Report TFD-88-2, Mechanical and Nuclear Engineering Department, Mississippi State University, 1988
16. Eckert, E. R. G.; Goldstein, R. J.: Measurements in Heat Transfer, 2nd edition, New York: McGraw-Hill 1976
17. Measurement Uncertainty, ANSI/ASME PTC 19.1.1985 Part 1, 1986
18. Coleman, H. W.; Steele, W. G.: Experimentation and uncertainty analysis for engineers. New York: Wiley 1989
19. Lin, T. C.; Bywater, R. J.: The evaluation of selected turbulence models for high-speed rough wall boundary layer calculations. AIAA paper 80-0132, 1980
20. Scaggs, W. F.; Taylor, R. P.; Coleman, H. W.: Measurement and prediction of rough wall effects on friction factors in turbulent pipe flow. Report TFD-88-1, Mechanical and Nuclear Engineering Department, Mississippi State University, 1988
21. Hosni, M. H.; Coleman, H. W.; Taylor, R. P.: Measurement and calculation of surface roughness effects on turbulent flow and heat transfer. Report TFD-89-1, Mechanical and Nuclear Engineering Department, Mississippi State University, 1989
22. Gatlin, B.; Hodge, B. K.: A generalized program for computing two-dimensional boundary layers on a personal computer. In: Numerical Heat Transfer with Personal Computers and Supercomputing. ASME HTD-Vol. 110 (1989) 25–30
23. Kays, W. M.; Crawford, M. E.: Convective heat and mass transfer. New York: McGraw-Hill 1980
24. Schultz-Grunow, F.: New frictional resistance law for smooth plates. NACA TM 986, Washington DC, 1941

R. P. Taylor, Professor
M. H. Hosni, Research Associate
J. W. Garner, Graduate Student
H. W. Coleman, Professor
Thermal & Fluid Dynamics Laboratory
Mechanical and Nuclear Engineering Department
Mississippi State University, MS, 39762, USA

Received May 22, 1990